Korean J. Chem. Eng., 33(3), 902-913 (2016)
DOI: 10.1007/s11814-015-0198-4

pISSN: 0256-1115
eISSN: 1975-7220

Synthesis of nanostructured adsorbent and dye adsorption modeling by an intelligent model for multicomponent systems

Niyaz Mohammad Mahmoodi†, Zahra Hosseinabadi-Farahani, and Hooman Chamani

Department of Environmental Research, Institute for Color Science and Technology, Tehran, Iran
(*Received 9 May 2015 • accepted 19 September 2015*)

Abstract−β-$Ni(OH)_2$ nanoparticle was synthesized and used as an adsorbent. The prepared adsorbent was characterized by scanning electron microscopy (SEM), field emission scanning electron microscopy (FESEM), Fourier transform infrared (FTIR) and X-ray diffraction (XRD). Least square support vector machine (LSSVM) as an intelligent model was applied for modeling of dye removal based on experimental data obtained from laboratory. The nanostructured adsorbent was used to remove three cationic dyes (BB41: Basic blue 41, BR18: Basic Red 18 and BR46: Basic Red 46) from single and binary systems at room temperature. The kinetics and isotherm of dye adsorption was studied. The effects of adsorbent dosage and initial dye concentration were elucidated. The kinetic studies showed that the adsorption data followed pseudo-second order kinetics model. The isotherm analysis indicates that the adsorption data can be represented by Langmuir in single systems. Based on graphical plots and the values of statistical parameter, LSSVM as an intelligent model is suitable for modeling of dye adsorption from single and binary systems.

Keywords: Nanostructured Adsorbent, Synthesis, Intelligent Modeling, Binary System, Dye Adsorption, Wastewater

INTRODUCTION

The control of water pollution has become a main issue in environmental science [1-6]. Due to large-scale production and extensive application, dyes are an important class of pollutants [7-14]. They are extensively used in many fields of advanced technology, such as in the textile industry, paper, leather tanning, food processing, plastics and cosmetics [15-19]. Most dyes are complex organic compounds that reduce penetration of sunlight into the water. A wide range of methods such as electrochemical oxidation, photocatalysis, and adsorption have been developed for the removal of dyes from wastewater [20-23]. Among these methods, adsorption with an inexpensive and efficient adsorbent is considered as a simple, flexible and economical technique. Adsorption also does not produce harmful [8]. Several materials including inorganic nanoparticles, polymers, and biomaterials (chitosan, enzyme, etc.), are used to remove dyes. Chitosan is the N-deacetylated derivative of chitin [24]. Enzymes can degrade dyes and other compounds such as sericin [25].

A literature review showed that the modeling of dye adsorption on β-$Ni(OH)_2$ using least square support vector machine (LSSVM) for binary systems was not studied. In previous study, LSSVM was used for modeling of enzymatic dye degradation [3]. In this work, β-$Ni(OH)_2$ nanostructure was synthesized and used to remove basic dyes from single and binary systems. Basic Blue 41 (BB41), Basic Red 18 (BR18) and Basic Red 46 (BR46) were used. The structure of adsorbent was confirmed by Fourier transform infrared (FTIR), scanning electron microscopy (SEM), field emission scanning electron microscopy (FESEM) and X-ray diffraction (XRD). The kinetics and isotherm of dye adsorption in both systems were studied. The effects of operational parameters were evaluated. In addition, LSSVM was applied for dye removal modeling based on experimental data obtained from laboratory.

EXPERIMENTAL

1. Materials and Methods

Basic Blue 41, Basic Red 18 and Basic Red 46 were used as model

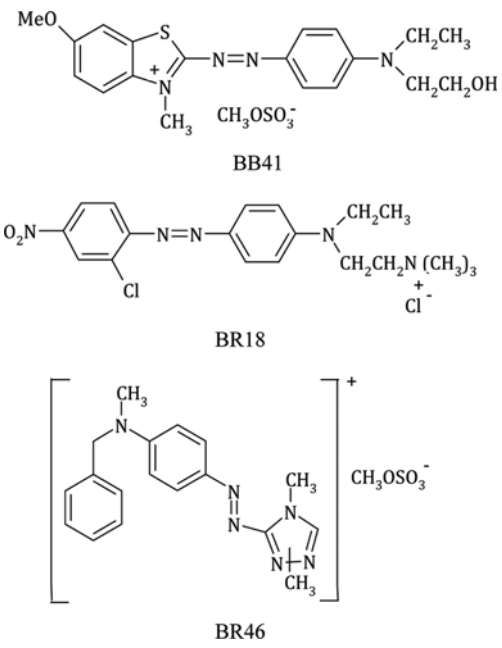

Fig. 1. The chemical structure of dyes.

†To whom correspondence should be addressed.
E-mail: mahmoodi@icrc.ac.ir, nm_mahmoodi@aut.ac.ir, nm_mahmoodi@yahoo.com

dyes. The chemical structure of the dyes is shown in Fig. 1. Nickel sulfate and sodium hydroxide pellet were obtained from Merck (Germany).

2. Synthesis of β-Ni(OH)$_2$

Sodium hydroxide (1 g) was added to 90 mL deionized water. The solution was stirred magnetically to dissolve sodium hydroxide. Then 1 g Nickel Sulfate. $6H_2O$ powder was poured into the bottle. The obtained solution was green and stirred for 30 min at room temperature. The bottle was then sealed and placed in an oven at 120 °C for 24 hours. The supernatant was decanted and green solid residue was washed four times with deionized water. The resulting solid was dried in an oven at 120 °C. The functional groups of prepared adsorbent were studied using FTIR (Perkin-Elmer spectrophotometer Spectrum One) in the range 4,000-450 cm^{-1}. The morphological structure of β-Ni(OH)$_2$ was examined by SEM (LEO 1455VP scanning electron microscope) and FESEM (Mira 3-XMU). The powder X-ray diffraction (XRD) measurement was recorded by XRD model Siemens D-5000 diffractometer with Cu K_α radiation at room temperature.

3. Adsorption Procedure

Dye removal from aqueous solution by the β-Ni (OH)$_2$ nanostructure involved the following experimental procedure: 250 mL of dye solution was mixed with the adsorbent at speed of 200 rpm and room temperature for 60 min. The change in the absorbance of all solution samples was monitored and determined at certain time intervals during the adsorption process. At the end of dye adsorption process, samples were centrifuged and their absorbance was determined. UV-Vis spectrophotometer (Perkin-Elmer Lambda 25 Spectrophotometer) was used for absorbance measurement of samples. Maximum wavelength used for determination of residual concentration was 488, 531 and 605 nm for BR18, BR46 and BB41, respectively.

The effect of adsorbent dosage on dye removal from single and binary systems was investigated by contacting 250 mL of dye solution with initial dye concentration of 20 mg/L at 25 °C for 60 min. Different amounts of β-Ni (OH)$_2$ nanostructure (0.05-1.2 g/L) were applied.

The effect of initial dye concentration (20-80 mg/L) on dye removal from both systems was investigated by contacting 250 mL of dye solution with β-Ni (OH)$_2$ nanostructure at 25 °C for 60 min.

RESULT AND DISCUSSION

1. Characterization

Fig. 2 shows the FTIR spectrum of β-Ni(OH)$_2$ nanostructure. The peak at 3,643 cm^{-1} is assigned to the stretching vibrational mode (ν_{OH}) of non-hydrogen bonded hydroxyl groups in the nickel hydroxide. The broad band at 3,444 cm^{-1} corresponds to the stretching mode of hydrogen bonded hydroxyl groups in the structure. The peak at 1,636 cm^{-1} indicates that Ni(OH)$_2$ contains traces of water. The peak at 534 cm^{-1} is attributed to the in-plane deformation vibration of water (ν_{OH}) and the shoulder at 467 cm^{-1} to the stretching vibration of Ni-OH ($\nu_{Ni\text{-}OH}$) [26-28].

SEM and FESEM are useful for characterizing the physical properties and surface morphology of the adsorbent surface. In adsorbent images, the size and shape of particles can be detected (Fig. 3). The results showed that the adsorbent has nanosize (<80 nm).

The XRD pattern of β-Ni (OH)$_2$ nanostructure is shown in Fig. 4. All diffraction peaks can be indexed to the pure hexagonal phase of β-Ni(OH)$_2$ (JCPDS, file No. 01-1047). No peak of impurity is

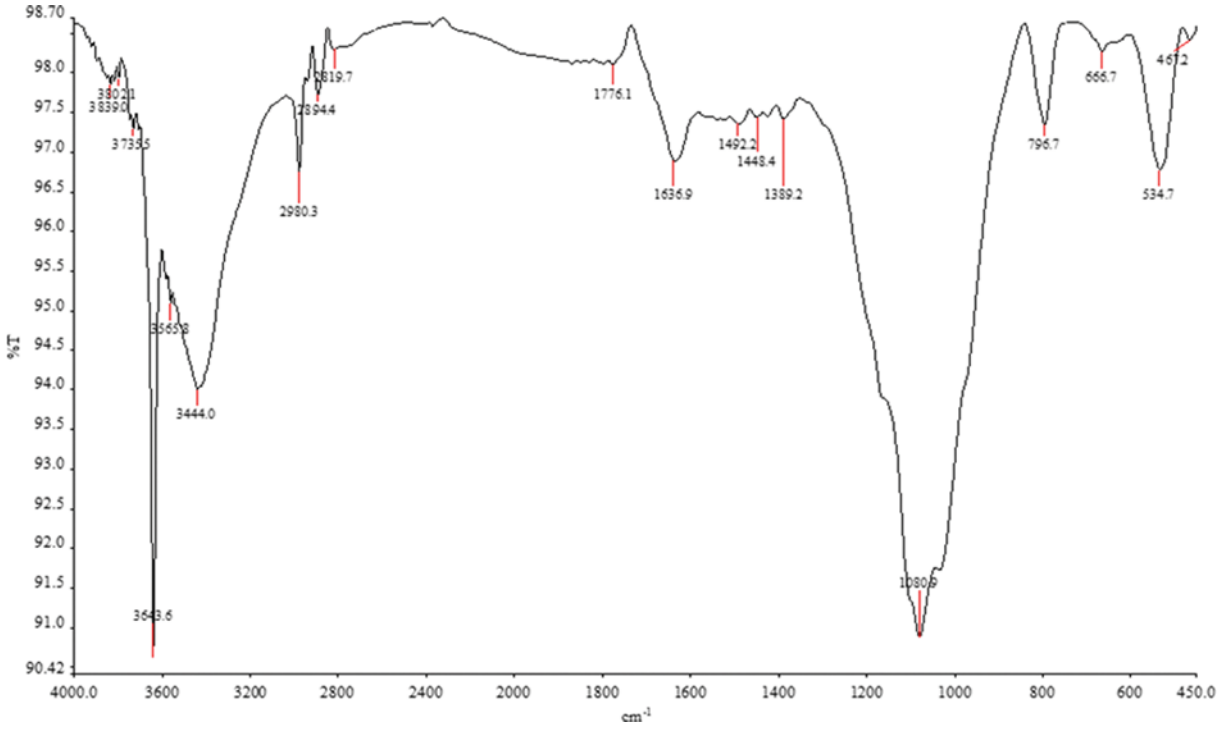

Fig. 2. FTIR spectrum of β-Ni (OH)$_2$ nanostructure.

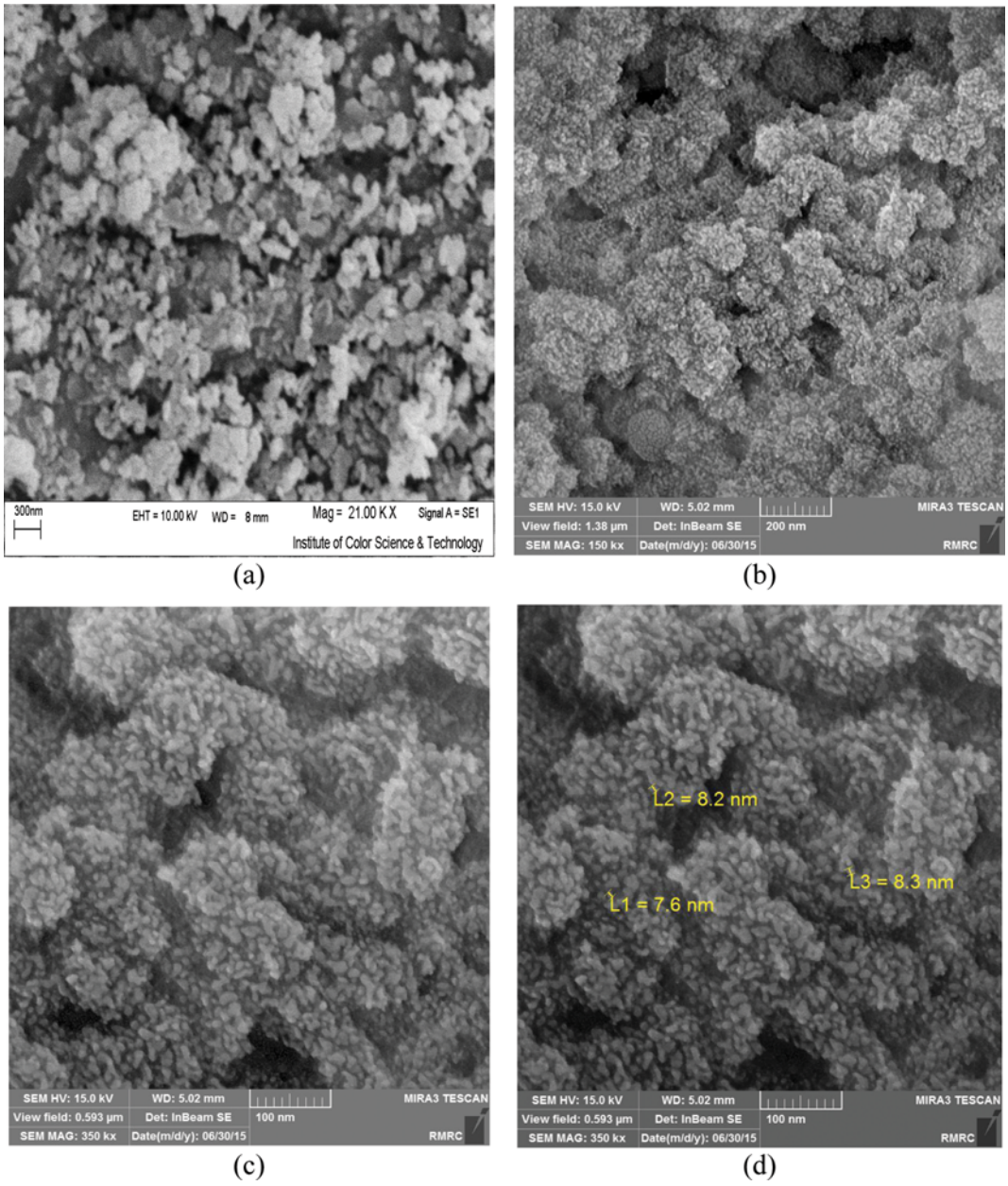

Fig. 3. Images of β-Ni $(OH)_2$ nanostructured adsorbent (a) SEM and (b), (c) and (d) FESEM.

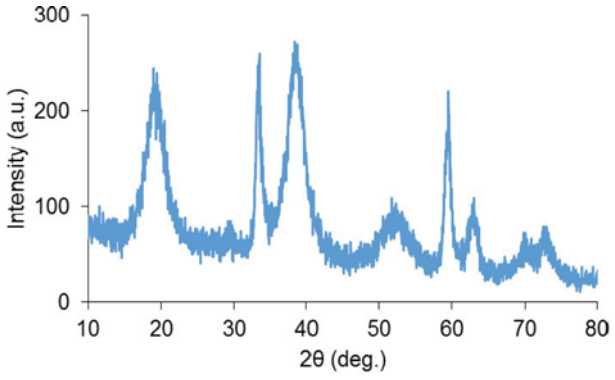

Fig. 4. X-ray diffraction (XRD) pattern of β-Ni $(OH)_2$ nanostructure.

observed [28-32].

2. Adsorption Kinetics

Several models can be used to express the mechanism of adsorption onto an adsorbent. To investigate the mechanism of adsorption, characteristic constants of sorption were determined using pseudo-first order, pseudo-second order, and intraparticle diffusion model [22,23].

The linear form of pseudo-first order model is:

$$\log(q_e - q_t) = \log(q_e) - (k_1/2.303)t \quad (1)$$

where q_e, q_t and k_1 are the adsorbed dye at equilibrium (mg/g), the amount of adsorbed dye at time t (mg/g) and the equilibrium rate constant of pseudo-first order kinetics (1/min), respectively.

The linear form of pseudo-second order model is illustrated as:

$$t/q_t=1/k_2q_e^2+(1/q_e)t \quad (2)$$

where k_2 is the equilibrium rate constant of pseudo second order kinetics (g/mg min).

The possibility of intraparticle diffusion resistance affecting adsorption was explored by using the intraparticle diffusion model as:

$$q_t=k_pt^{1/2}+I \quad (3)$$

where k_p and I are the intraparticle diffusion rate constant and intercept, respectively.

To understand the applicability of the pseudo-first order, pseudo-

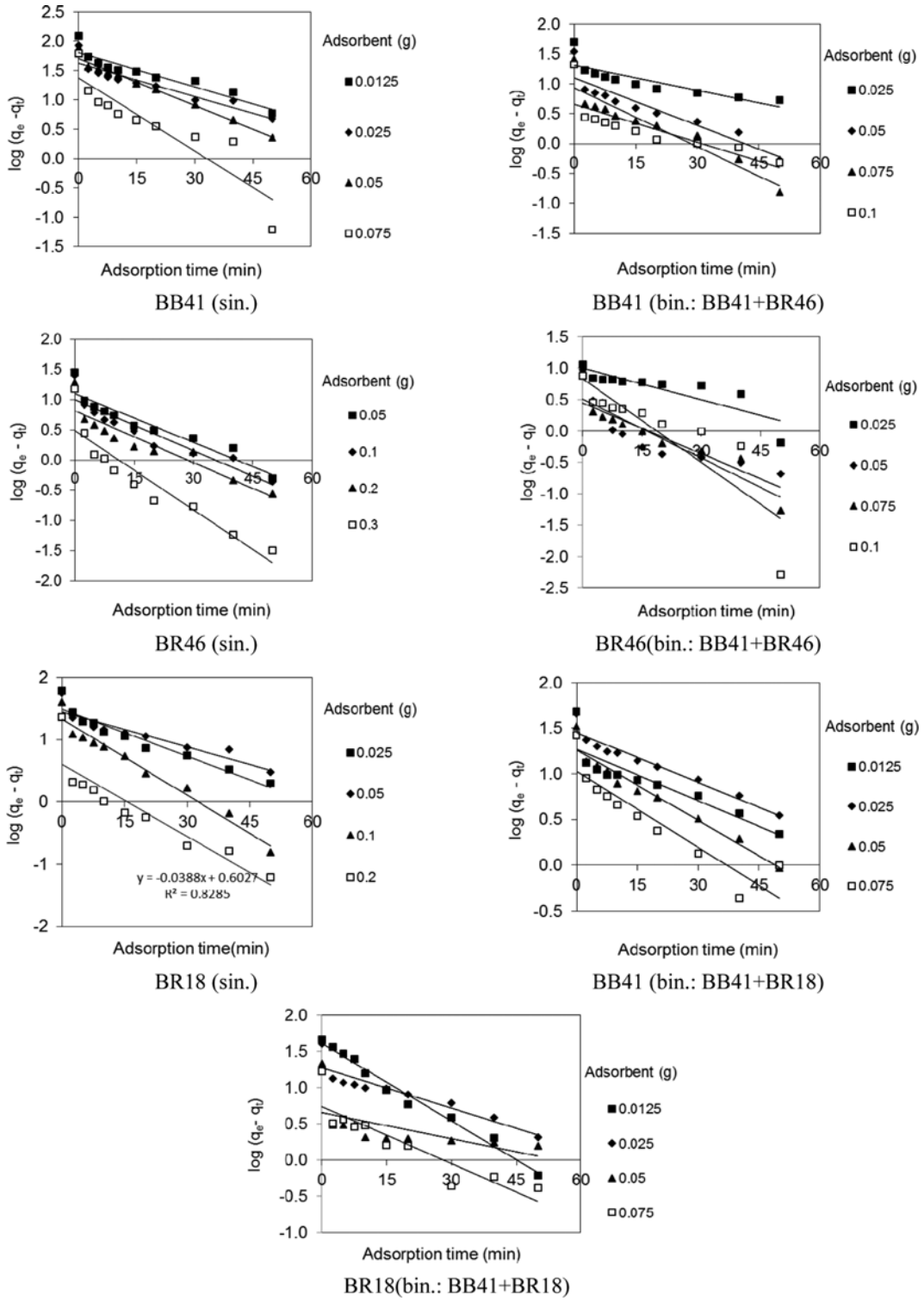

Fig. 5. Pseudo-first order kinetics of dye removal by adsorbent from single (sin.) and binary (bin.) systems.

second order and intraparticle diffusion models for dye adsorption onto adsorbent at different amount of adsorbent from single (sin.) and binary (bin.) systems, linear plots of $\log(q_e - q_t)$ versus contact time (t), t/q_t versus contact time(t) and q_t against $t^{1/2}$ were plotted (Fig. 5 to 7). The values of k_1, k_2, k_p, I, R^2 (correlation coefficient values) and the calculated q_e ($(q_e)_{Cal.}$) are shown in Table 1.

The R^2 values show that dye adsorption by β-$Ni(OH)_2$ does not follow pseudo-first order and intraparticle diffusion kinetics. The linearity of the t/q_t against t and the R^2 values show that the kinetics of dye removal follows pseudo-second order model.

3. Adsorption Isotherm

The adsorption isotherm studies the pollutant adsorption mechanism on to the adsorbent. Several isotherms such as Langmuir, Freundlich and Temkin models were studied [22,23,33].

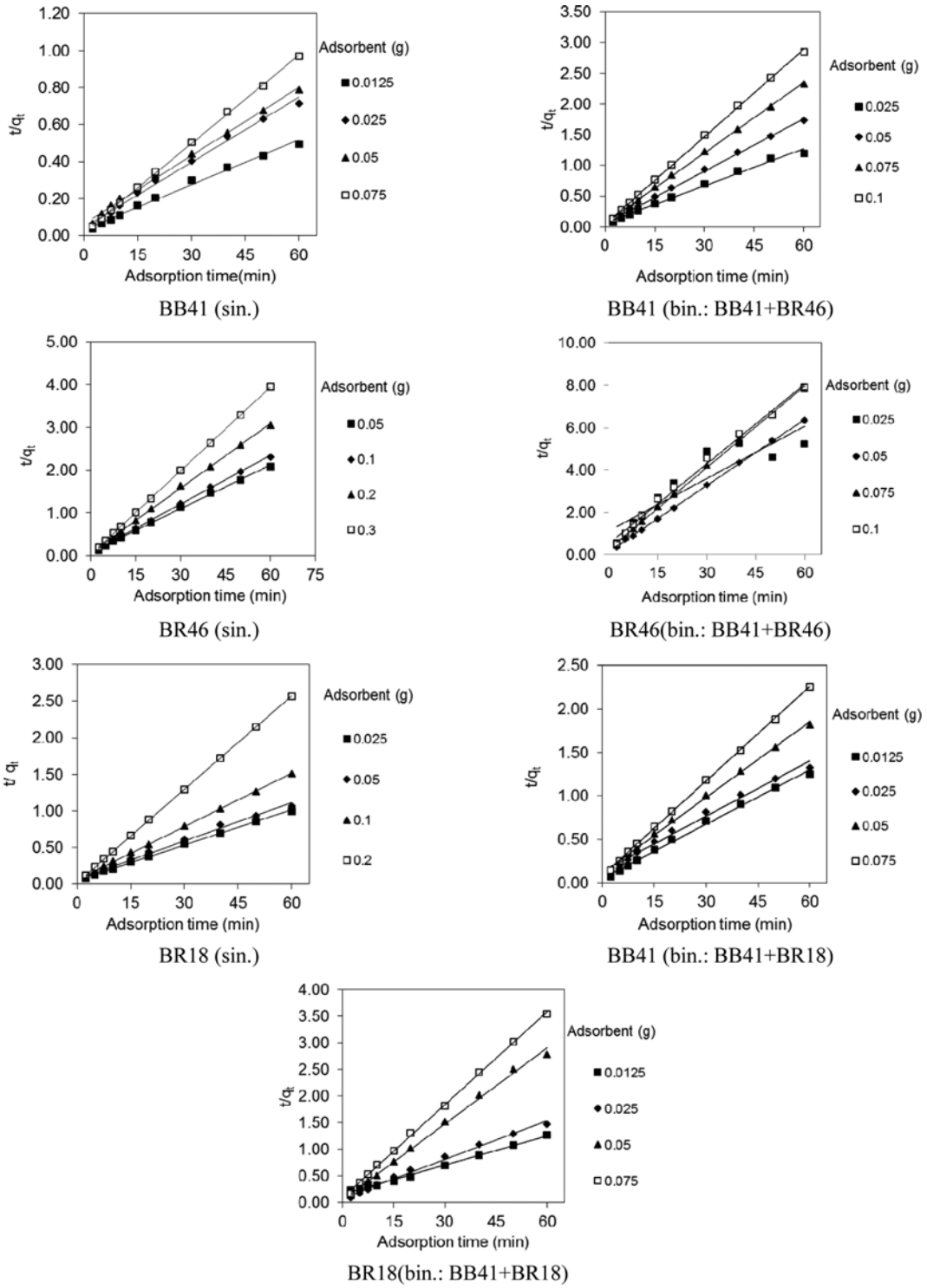

Fig. 6. Pseudo-second order kinetics of dye removal by adsorbent from single (sin.) and binary (bin.) systems.

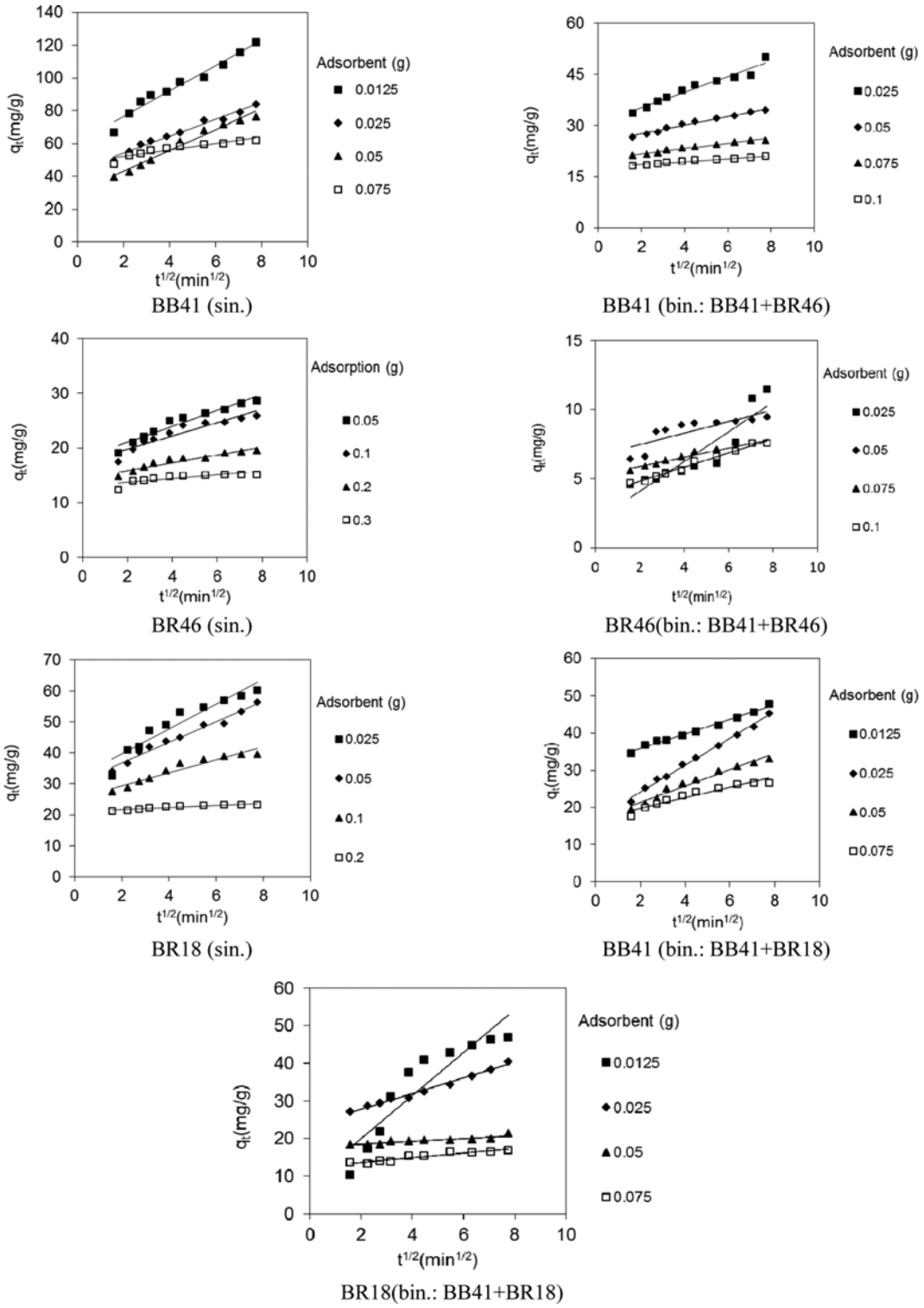

Fig. 7. Intraparticle diffusion kinetics of dye removal by adsorbent from single (sin.) and binary (bin.) systems.

The Langmuir isotherm assumes that adsorption takes place at specific sites of the adsorbent surface:

$$C_e/q_e=1/K_LQ_0+C_e/Q_0 \quad (4)$$

where C_e, K_L and Q_0 are the equilibrium concentration of dye solution (mg/L), the Langmuir constant (L/g) and the maximum adsorption capacity (mg/g), respectively.

Isotherm data were tested with Freundlich isotherm that can be expressed by:

$$\log q_e=\log K_F+(1/n)\log C_e \quad (5)$$

where K_F is adsorption capacity at unit concentration and 1/n is

Table 1. Linearized kinetics coefficients of dye removal at different adsorbent dosages from single and binary systems

	Dye		Adsorbent (g)	$(q_e)_{Exp}$	Pseudo-first order			Pseudo-second order			Intraparticle diffusion		
					$(q_e)_{Cal.}$	k_1	R^2	$(q_e)_{Cal.}$	k_2	R^2	k_p	I	R^2
Single system	BB41		0.0125	121.68	65.21	0.0454	0.8821	125.00	0.0019	0.9919	7.8104	60.693	0.9673
			0.025	83.99	42.26	0.0438	0.8758	85.47	0.0031	0.9938	5.0987	44.128	0.9821
			0.05	76.32	51.56	0.0622	0.9788	81.97	0.0023	0.9964	6.3648	30.277	0.9752
			0.075	61.87	23.55	0.0960	0.8229	62.89	0.0130	0.9996	1.9702	48.106	0.8648
	BR46		0.05	28.66	12.74	0.0615	0.8972	29.33	0.0139	0.9987	1.4640	18.040	0.9458
			0.1	25.88	9.97	0.0643	0.8773	26.39	0.0196	0.9995	1.2123	17.348	0.8872
			0.2	19.59	6.56	0.0656	0.8572	19.88	0.0325	0.9993	0.7140	14.471	0.9113
			0.3	15.19	3.12	0.1009	0.8675	15.34	0.1146	1	0.3362	13.017	0.6610
	BR18		0.025	60.40	31.07	0.0580	0.9260	62.50	0.0048	0.9987	4.0250	31.586	0.9122
			0.05	56.44	28.16	0.0433	0.8629	57.14	0.0047	0.9931	3.3491	30.052	0.9785
			0.1	39.64	21.43	0.0940	0.9663	41.15	0.0104	0.9994	2.0999	25.215	0.9296
			0.2	23.36	4.01	0.0894	0.8285	23.53	0.0848	1	0.3492	20.976	0.8849
Binary system	BB41+BR18	BB41	0.0125	47.86	18.52	0.0431	0.7963	48.08	0.0082	0.9958	1.9687	31.899	0.9874
			0.025	45.30	28.48	0.0419	0.9382	47.17	0.0035	0.9888	3.6159	16.944	0.9939
			0.05	33.00	18.25	0.0594	0.9480	34.36	0.0078	0.9977	2.2094	16.921	0.9654
			0.075	26.63	10.74	0.0643	0.8326	27.62	0.0158	0.9995	1.4036	17.009	0.9251
		BR18	0.0125	46.92	41.26	0.0822	0.9818	54.95	0.0020	0.9934	5.7252	8.493	0.8648
			0.025	40.56	18.99	0.0426	0.8469	41.15	0.0069	0.9926	2.0805	23.637	0.9865
			0.05	21.51	4.56	0.0276	0.3763	20.96	0.0433	0.9965	0.3887	17.724	0.7976
			0.075	16.94	5.52	0.0606	0.8035	17.21	0.0346	0.9991	0.6134	12.454	0.9099
	BB41+BR46	BB41	0.025	50.16	20.10	0.0320	0.6961	49.62	0.0073	0.9922	2.2953	30.662	0.9537
			0.05	34.50	12.37	0.0608	0.8588	35.09	0.0157	0.9990	1.2902	24.939	0.9765
			0.075	25.75	8.63	0.0755	0.8783	26.18	0.0270	0.9994	0.7801	20.079	0.9798
			0.1	21.08	4.50	0.0488	0.6582	21.10	0.0482	0.9994	0.4306	17.683	0.9766
		BR46	0.025	11.48	9.88	0.0380	0.7159	12.11	0.0061	0.8351	1.068	1.957	0.8293
			0.05	9.46	2.80	0.0615	0.7414	9.59	0.0724	0.9995	0.4184	6.620	0.6724
			0.075	7.61	3.25	0.0721	0.8819	7.78	0.0631	0.9989	0.3268	5.248	0.9648
			0.1	7.57	6.85	0.1023	0.7491	7.97	0.0290	0.9940	0.5079	3.803	0.9851

Table 2. Linearized isotherm coefficients of dye removal at different adsorbent dosages from single and binary systems

System		Langmuir			Freundlich			Temkin		
		Q_0	K_L	R^2	K_F	1/n	R^2	K_T	B_1	R^2
Single system						BB41				
		120.48	0.4462	0.8754	54.92	0.2382	0.7648	12.11	20.53	0.6785
						BR18				
		74.07	0.3230	0.9950	21.40	0.4176	0.9833	3.09	16.33	0.9855
						BR46				
		33.33	0.3896	0.9963	12.66	0.3093	0.9908	5.33	66.54	0.9885
Binary system	BB41+BR18					BB41				
		66.84	0.3566	0.9827	20.82	0.4341	0.9732	2.96	15.79	0.9663
						BR18				
		25	0.0931	0.4937	1.44	2.1751	0.7637	3.42	65.16	0.7835
	BB41+BR46					BB41				
		170	0.0831	0.6513	14.19	0.7833	0.9795	1.30	25.94	0.9314
						BR46				
		17	0.0419	0.5288	2.66	1.5126	0.9039	4.25	14.03	0.8960

adsorption intensity.

The Temkin isotherm is given as:

$$q_e = B_1 \ln K_T + B_1 \ln C_e \quad (6)$$

where K_T is the equilibrium binding constant (L/mol) corresponding to the maximum binding energy and the constant B_1 (RT/b) is related to the heat of adsorption. In addition, R and T are the gas constant (8.314 J/mol K) and the absolute temperature (K), respectively.

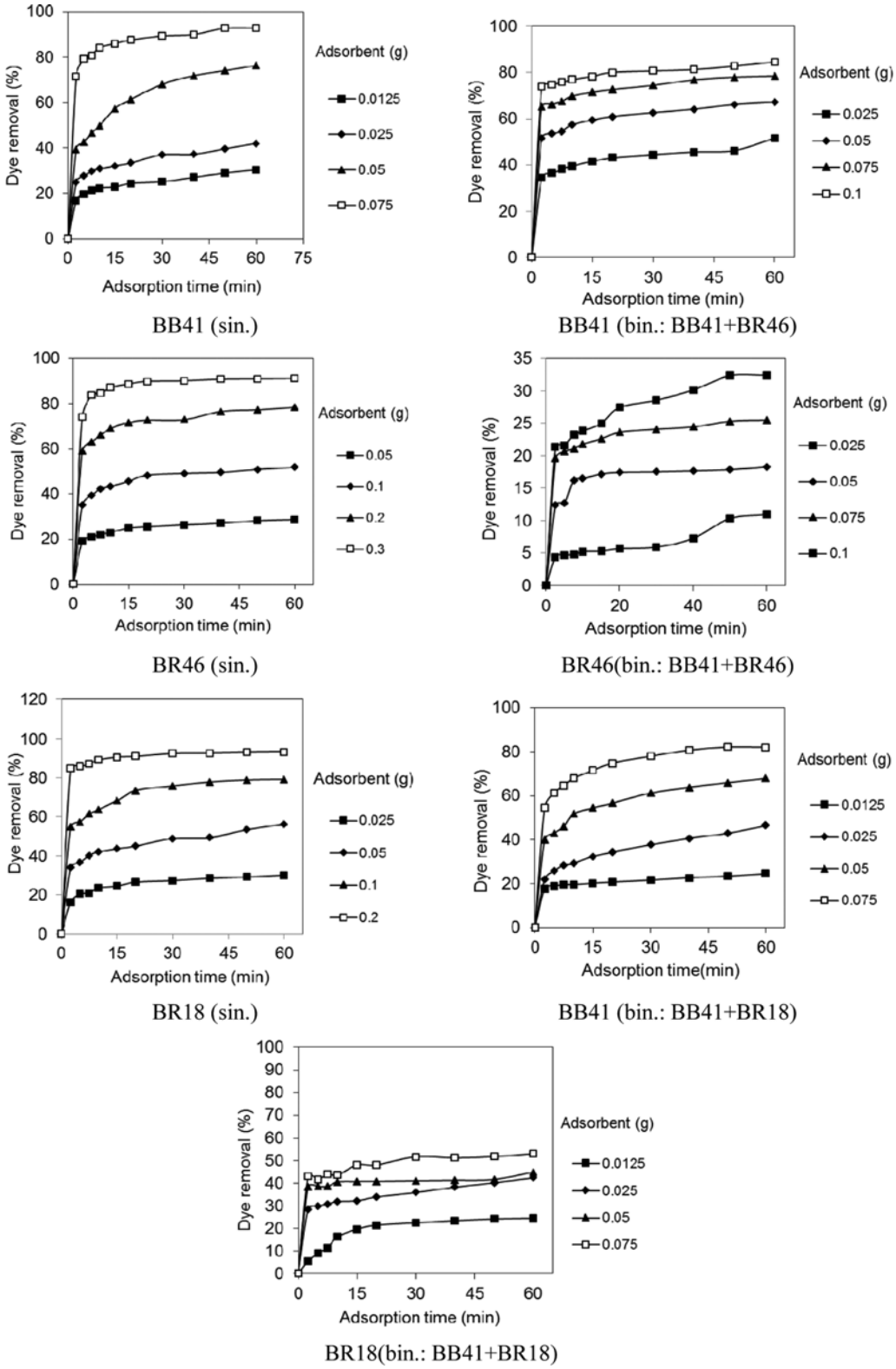

Fig. 8. The effect of adsorbent dosage on dye removal by adsorbent from single (sin.) and binary (bin.) systems.

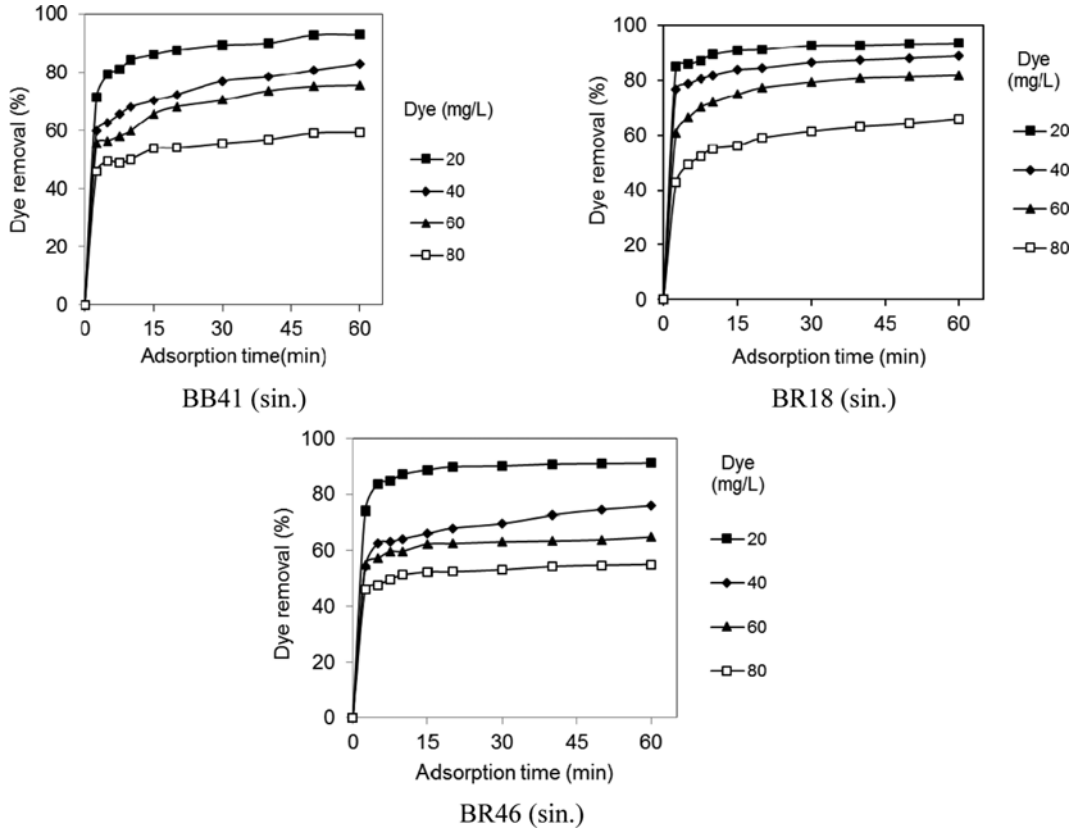

Fig. 9. The effect of dye concentration on dye removal by adsorbent from single (sin.) systems.

To study the applicability of the Langmuir, Freundlich and Temkin isotherms for the dye adsorption onto β-$Ni(OH)_2$ from single (sin.) and binary (bin.) systems at different adsorbent dosages, linear plots of C_e/q_e against C_e, log q_e versus log C_e and q_e versus ln C_e were plotted. The values of Q_0, K_L, K_F, 1/n, K_T, B_1 and R^2 are shown in Table 2.

The R^2 values of single systems show that the dye removal isotherms follow Langmuir model (Table 2) because the dye adsorption onto β-$Ni(OH)_2$ takes place at specific homogeneous sites and a one layer adsorption.

4. Effect of Operational Parameter on Dye Removal

The plots of dye removal (%) versus time (min) at different β-$Ni(OH)_2$ dosages are shown in Fig. 8. The dye removal percent increases by increasing adsorbent dosage. The total adsorbent surface area available to the dye increases with increasing the adsorbent dosage. However, increasing adsorption sites available to the dyes is not proportionate to the increase in adsorbent dosage due to the overlapping or aggregation of adsorption sites, which results in the decrease of capacity expressed in milligrams adsorbed per gram of adsorbent.

The plots of dye removal (%) versus time (min) at different dye concentrations are shown in Fig. 9. The dye adsorption onto the adsorbent increases with an increase in the initial dye concentration of solution if the amount of adsorbent is kept unchanged, due to the increase in the driving force of the concentration gradient with the higher initial dye concentration. Dye removal using the adsorbent at 20, 40, 60 and 80 mg/L dye concentration was 92, 83, 75 and 59% for BB41, 93, 88, 81 and 65% for BR18 and 91, 75, 64 and 55% for BR46, respectively.

5. Dye Removal Modeling

The support vector machine (SVM) approach was presented by Vapnik as a potential alternative to conventional artificial neural network [34,35]. In other words, it is a supervised learning algorithm for classification and nonlinear function estimation [36-40].

The SVM builds a separating hyper-surface for input space. It maps the input patterns into a higher dimensional feature space using nonlinear mapping, and a separating hyper-plane with maximum margin is built [3,35,41-44]. Consider the following training samples:

$$((x_1, y_1), (x_2, y_2), \ldots, (x_n, y_n)) \tag{7}$$

where input data (x_i) are members of R^n and output data (y_i) are members of R with class label −1 for class 1 and class label 1 for class 2. If this data sample is linearly separable in the feature space, the following regression model can be constructed [3,43,44]:

$$y=w^T\varphi(x)+b \tag{8}$$

where w, $\varphi(x)$ and b are weight vector, nonlinear function that maps x from low dimensional space into *n*-dimensional feature space, and bias terms, respectively. If the data of two classes are separable, one can say [3,43]:

$$\begin{cases} w^T\varphi(x_k)+b\geq+1, \text{ if } y_k=+1 \\ w^T\varphi(x_k)+b\leq-1, \text{ if } y_k=-1 \end{cases} \tag{9}$$

which is equivalent to [3,43]:

$$y_k[w^T\varphi(x_k)+b]\geq+1,\ k=1,\ 2,\ \ldots,\ N \tag{10}$$

The development of linear SVM to non-separable one was made by Cortes and Vapnik [35], which is done by introducing additional slack variables into Eq. (10) as follows [3,43]:

$$\begin{cases} y_k[w^T\varphi(x_k)+b]\geq 1-\zeta_k,\ k=1,\ \ldots,\ N \\ \zeta_k\geq 0 \text{ for } k=1,\ \ldots,\ N \end{cases} \tag{11}$$

The generalized optimal separating hyper-plane is determined by the vector w, that minimizes the functional [3,43]:

$$\text{Cost function}=\frac{1}{2}w^Tw+\frac{\gamma}{2}\sum_{i=1}^{N}\zeta_i^p \tag{12}$$

subject to the constraint:

$$y_k[w^T\varphi(x_k)+b]\geq 1-\zeta_k,\ k=1,\ \ldots,\ N \tag{13}$$

where γ is a positive constant that determines the tradeoff between the maximum margin and the minimum classification error [3, 43-45].

LSSVM is a modified version of SVM developed by Suykens and Vandewalle for simplifying and improving [3,44]. Unlike SVM, LSSVM solution is obtained by solving a linear set of equations instead of solving the above quadratic programing problem [3,43, 44,46] because of working with equality constraints instead of inequality ones. LSSVM can be trained by minimizing the following cost function [3,43,47]:

$$\text{Cost function}=\frac{1}{2}w^Tw+\frac{\gamma}{2}\sum_{i=1}^{N}\zeta_k^2 \tag{14}$$

subject to the following constraint:

$$y_k[w^T\varphi(x_k)+b]=1-\zeta_k,\ k=1,\ \ldots,\ N \tag{15}$$

The Lagrangian for this problem is as follows [3,43,44]:

$$L(w,\ b,\ \zeta,\ \alpha)=\frac{1}{2}w^Tw+\frac{\gamma}{2}\sum_{k=1}^{N}\zeta_k^2 - \sum_{k=1}^{N}\alpha_k(y_k[w^T\varphi(x_k)+b]-1+\zeta_k) \tag{16}$$

where α_k are Lagrange multipliers.

To solve the problem, the derivatives of Eq. (16) should be equated to zero. Therefore, the following equations are obtained [43]:

$$\begin{cases} \dfrac{\partial L}{\partial w}=0\Rightarrow w=\sum_{k=1}^{N}\alpha_k y_k\varphi(x_k) \\ \dfrac{\partial L}{\partial b}=0\Rightarrow \sum_{k=1}^{N}\alpha_k y_k=0 \\ \dfrac{\partial L}{\partial \zeta_k}=0\Rightarrow \alpha_k=\gamma\zeta_k,\ k=1,\ \ldots,\ N \\ \dfrac{\partial L}{\partial \alpha_k}=0\Rightarrow y_k[w^T\varphi(x_k)+b]-1+\zeta_k=0,\ k=1,\ \ldots,\ N \end{cases} \tag{17}$$

By defining Eq. (18) and eliminating w and ζ, the optimization problem is transformed to Eq. (19) [3,43,44]:

$$\begin{cases} z^T=[\varphi(x_1)^Ty_1;\ \ldots;\ \varphi(x_N)^Ty_N] \\ Y=[y_1;\ \ldots;\ y_N] \\ 1_v=[1;\ \ldots;\ 1] \\ \zeta=[\zeta_1;\ \ldots;\ \zeta_N] \\ \alpha=[\alpha_1;\ \ldots;\ \alpha_N] \end{cases} \tag{18}$$

$$\begin{bmatrix} 0 & 1_N^T \\ 1_N & \Omega+\gamma^{-1}I_N \end{bmatrix}\begin{bmatrix} b \\ \alpha \end{bmatrix}=\begin{bmatrix} 0 \\ Y \end{bmatrix} \tag{19}$$

where I_N is N×N identity matrix, and $\Omega\in R^{N\times N}$ is the kernel matrix defined as follows:

$$W_{ij}=\varphi(x_i)\varphi(x_j)=K(x_i,\ x_j) \tag{20}$$

where $K(x_i, x_j)$ is kernel function. RBF is one of most widely used kernel function which can be defined as follows:

$$K(x_i, x_j)=\exp(-\|x_i-x_j\|^2/\sigma^2) \tag{21}$$

where σ^2 is the squared variance of Gaussian function.

In the present study, there were 70 and 40 experimental data sets for each dye in single and binary systems, respectively. 70% of all experimental data sets were applied for training and the rest used as testing data. To have similar domains, all input and output variables were normalized between −1 and +1 by using Eq. (23):

$$x_{norm}=2\frac{x_{orig}-x_{min}}{x_{max}-x_{min}}-1 \tag{22}$$

where x_{orig} and x_{norm} are original and normalized values of variable x_{orig}, respectively. x_{min} and x_{max} are extreme values of x_{orig}. Results were converted to original state after modeling. Table 3 illustrates ranges of experimental data.

Table 3. Ranges of experimental data

Variable	Range				
Input	BB41	BR18	BR46	BB41+BR18	BB41+BR46
Adsorbent dosage (g/L)	0.05-0.3	0.1-0.8	0.2-1.2	0.05-0.3	0.1-0.4
Initial dye concentration (mg/L)	20-80	20-80	20-80	20*	20*
Adsorption time (min)	2.5-60	2.5-60	2.5-60	2.5-60	2.5-60
Output					
Dye removal percent (%)	16.8-92.8	16.3-93.5	19.1-91.2	5.4-82.1	4.4-84.6

*Concentration of each dye=10 mg/L

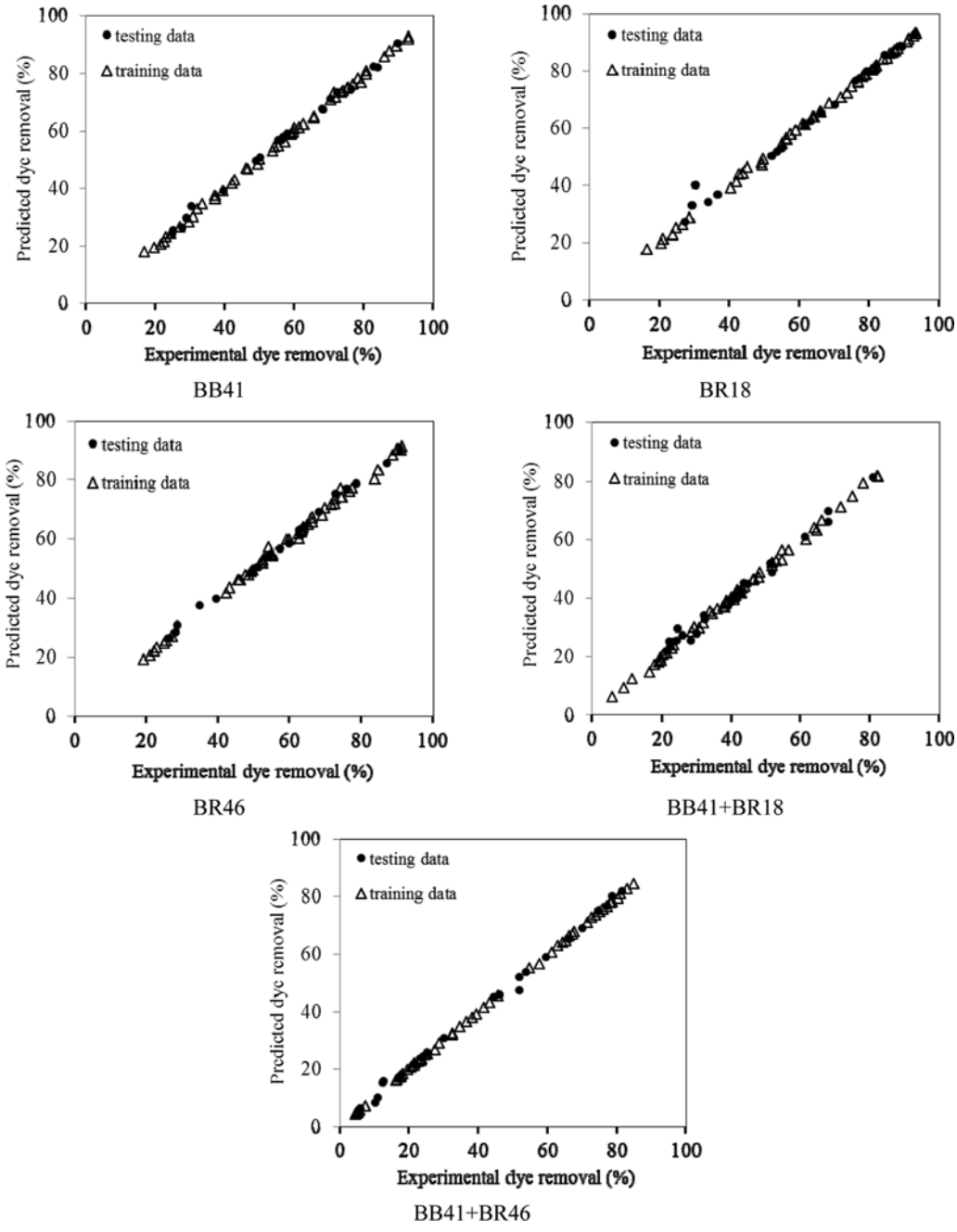

Fig. 10. LSSVM predicted dye removal vs. experimental dye removal for training and testing sets.

The free LSSVM toolbox (version 1.8, Suykens, Leuven, Belgium) in MATLAB R2009b environment was used to develop LSSVM for this study. In this modeling RBF kernel, was chosen as kernel function. The performance of LSSVM modeling was statically evaluated by the coefficient of determination (R^2) using following equation:

$$R^2 = 1 - \frac{\sum_{i=1}^{N}(y_{i,pred} - y_{i,exp})^2}{\sum_{i=1}^{N}(y_{i,exp} - \bar{y}_{exp})^2} \quad (23)$$

where N is the number of data points, $y_{i,pred}$ and $y_{i,exp}$ are the predicted and experimental y value of data point i, respectively, and $\bar{y}_{exp}$ is the average of experimental values.

As shown in Fig. 10, all data are well distributed in a narrow

Table 4. Statistical parameter for evaluation of modeling

Dye	R^2 train	R^2 test
BB41	0.9987	0.9969
BR18	0.9992	0.9867
BR46	0.9976	0.9965
BB41+BR18	0.9981	0.9851
BB41+BR46	0.9999	0.9969

area around the diagonal line, which indicates that predicted and experimental data have similar values to a large extent. On the other hand, the values of R^2 which are close to one confirm the reliability of LSSVM modeling for our system (Table 4).

CONCLUSIONS

β-$Ni(OH)_2$ nanostructured adsorbent was synthesized and its structure was confirmed by XRD, FTIR, SEM and FESEM. The adsorbent was applied to remove three cationic dyes from single and binary systems. The results showed that β-$Ni(OH)_2$ has a good ability to remove cationic dyes from both systems. It was found that dye adsorption kinetics and isotherm followed pseudo-second order model and Langmuir isotherm, respectively. Based on modeling data, LSSVM is suitable for modeling of adsorption process from single and binary systems.

REFERENCES

1. N. M. Mahmoodi, *J. Mol. Catal. A: Chem.*, **366**, 254 (2013).
2. N. M. Mahmoodi, *Mater. Res. Bull.*, **48**, 4255 (2013).
3. N. M. Mahmoodi, M. Arabloo and J. Abdi, *Water Res.*, **67**, 216 (2014).
4. A. Dalvand, M. Gholami, A. Joneidi, N. M. Mahmoodi, *Clean.*, **39**, 665 (2011).
5. N. M. Mahmoodi, *J. Ind. Eng. Chem.*, **27**, 251 (2015).
6. N. M. Mahmoodi, *Fiber. Polym.*, **15**, 273 (2014).
7. K. Singh and S. Arora, *Crit. Rev. Env. Sci. Technol.*, **41**, 807 (2014).
8. E. Forgacs, T. Cserhati and G. Oros, *Environ. Int.*, **30**, 953 (2004).
9. K. B. Narayanan and H. H. Park. *Korean J. Chem. Eng.*, **32**, 1273 (2015).
10. F. Huang, M. Luo, L. Cui and G. Wu, *Korean J. Chem. Eng.*, **32**, 268 (2015).
11. X. Tang, Y. Li, R. Chen, F. Min, J. Yang and Y. Dong, *Korean J. Chem. Eng.*, **32**, 125 (2015).
12. T. Vidhyadevi, M. Arukkani, K. Selvaraj, P. M. Periyaraman, R. Lingam and S. Subramanian, *Korean J. Chem. Eng.*, **32**, 650 (2015).
13. K. Mahmoudi, K. Hosni, N. Hamdi and E. Srasra, *Korean J. Chem. Eng.*, **32**, 274 (2015).
14. A. Mehmood, S. Bano, A. Fahim, R. Parveen and S. Khurshid, *Korean J. Chem. Eng.*, **32**, 882 (2015).
15. G. K. Ramesha, A. V. Kumara, H. B. Muralidhara and S. Sampath, *J. Colloid Interface Sci.*, **361**, 270 (2011).
16. H. Sun, L. Cao and L. Lu, *Nano Res.*, **4**, 550 (2011).
17. H. Parab, M. Sudersanan, N. Shenoy, T. Pathare and B. Vaze, *Clean.*, **37**, 963 (2009).
18. Y. Bulut and H. Aydin, *Desalination*, **194**, 259 (2006).
19. N. M. Mahmoodi, *J. Environ. Eng.*, **139**, 1368 (2013).
20. N. M. Mahmoodi, N. Y. Limaee, M. Arami, S. Borhany and M. Mohammad-Taheri, *J. Photochem. Photobiol. A: Chem.*, **189**, 1 (2007).
21. W. Dong, L. Zang and H. Li, *Appl. Mech. Mater.*, **361-363**, 760 (2013).
22. N. M. Mahmoodi, *Environ. Monit. Assess.*, **86**, 5595 (2014).
23. N. M. Mahmoodi, B. Hayati, M. Arami and H. Bahrami, *Desalination*, **275**, 93 (2011).
24. M. Ranibar-Mohammadi, M. Arami, H. Bahrami, F. Mazaheri, N. M. Mahmoodi, *Colloid. Surf. B*, **76**, 397 (2010).
25. N. M. Mahmoodi, M. Arami, F. Mazaheri and S. Rahimi, *J. Clean. Prod.*, **18**, 146 (2010).
26. N. Dharmaraj, P. Prabu, S. Nagarajan, C. H. Kim, J. H. Park and H. Y. Kim, *Mater. Sci. Eng., B.*, **128**, 111 (2006).
27. L. A. Saghatforoush, M. Hasanzadeh, S. Sanat and, R. Mehdizadeh, *Bull. Korean Chem. Soc.*, **33**, 2613 (2012).
28. F. Motahari, M. R. Mozdianfard, F. Soofivand and M. Salavati-Niasari, *RSC Adv.*, **4**, 27654 (2014).
29. D. P. Dubal, S. H. Lee and W. B. Kim, *J. Mater. Sci.*, **47**, 3817 (2012).
30. P. Zhang, X. Ma, K. Wang, Z. Tao, T. Liu and L. Yang, *Micro Nano Lett.*, **7**, 505 (2012).
31. B. Cheng, Y. Le, W. Cai and J. Yu, *J. Chin. Chem. Soc.*, **185**, 889 (2012).
32. M. Meyer, A. Bee, D. Talbot, V. Cabuil, J. M. Boyer, B. Repetti and R. Garrigos, *J. Colloid Interface Sci.*, **277**, 309 (2004).
33. N. M. Mahmoodi, *J. Environ. Eng.*, **139**, 1382 (2011).
34. E. Byvatov, U. Fechner, J. Sadowski and G. Schneider, *J. Chem. Inf. Comput. Sci.*, **43**, 1882 (2003).
35. C. Cortes, V. Vapnik and Support-Vector Networks, *Machine Learning.*, **20**, 273 (1995).
36. H. Safari, A. Shokrollahi, M. Jamialahmadi, M. H. Ghazanfari, A. Bahadori and S. Zendehboudi, *Fluid Phase Equilib.*, **374**, 48 (2014).
37. G. Moser and S. B. Serpico, *IEEE Geoscience and Remote Sensing Letters*, **6**, 448 (2009).
38. J. A. K. Suykens, *European J. Control.*, **7**, 311 (2001).
39. S. Rafiee-Taghanaki, M. Arabloo, A. Chamkalani, M. Amani, M. H. Zargari and M. R. Adelzadeh, *Fluid Phase Equilib.*, **346**, 25 (2013).
40. A. Baylar, D. Hanbay and M. Batan, *Expert Systems with Applications.*, **36**, 8368 (2009).
41. S. R. Amendolia, G. Cossu, M. Ganadu, B. Golosio, G. Masala and G. M. Mura, *Chemometr. Intell. Lab.*, **69**, 13 (2003).
42. A. Bazzani, A. Bevilacqua, D. Bollini, R. Brancaccio, R. Campanini, N. Lanconelli, A. Riccardi and D. Romani, *Phys. Med. Biol.*, **46**, 1651 (2001).
43. J. A. Suykens, T. Van Gestel, J. De Brabanter, B. De Moor and J. Vandewalle, *Least squares support vector machines*, World Scientific Pub. Co., Singapore (2002).
44. J. A. K. Suykens and J. Vandewalle, *Neural Process. Lett.*, **9**, 293 (1999).
45. E. D. Übeyli, *Expert Syst. Appl.*, **37**, 233 (2010).
46. A. Shokrollahi, M. Arabloo, F. Gharagheizi and A. H. Mohammadi, *Fuel*, **112**, 375 (2013).
47. A. Hemmati-Sarapardeh, A. Shokrollahi, A. Tatar, F. Gharagheizi, A. H. Mohammadi and A. Naseri, *Fuel*, **116**, 39 (2014).